ISSN 1063-7729, Astronomy Reports, 2007, Vol. 51, No. 3, pp. 234–244. © Pleiades Publishing, Ltd., 2007.
Original Russian Text © A.S. Gusev, V.I. Myakutin, F.Kh. Sakhibov, M.A. Smirnov, 2007, published in Astronomicheskiĭ Zhurnal, 2007, Vol. 84, No. 3, pp. 266–277.

Numerical Simulations of the Initial Mass Function and Star-Formation History Using a Grid of Evolutionary Models for Star Clusters

A. S. Gusev[1], V. I. Myakutin[2], F. Kh. Sakhibov[3,4], and M. A. Smirnov†[2]

[1] *Sternberg Astronomical Institute, Universitetskii pr. 13, Moscow, 119992 Russia*
[2] *Institute of Astronomy, Russian Academy of Sciences, Pyatnitskaya ul. 48, Moscow, 119017, Russia*
[3] *Giessen–Friedberg University of Applied Science, Wilhelm-Leuschner-Strasse 13, Friedberg, 61169 Germany*
[4] *Institute of Astrophysics, Academy of Sciences of Tajikistan, ul. Bukhoro 22, Dushanbe, 734670, Tajikistan*

Received April 10, 2006; in final form, October 12, 2006

Abstract—Numerical simulations are used to investigate the possibility of determining the physical properties of young star-forming complexes by finding the global minimum of a so-called deviation functional, which assigns each evolutionary model for a stellar population a number characterizing the deviation of the observed photometric properties from their model values. The deviation functional is calculated using a grid of evolutionary models computed at the Institute of Astronomy of the Russian Academy of Sciences. The parameters of the initial mass function (IMF) and the age corresponding to the global minimum of the deviation functional are strongly correlated with the IMF and age of the test model. The accuracy of the parameters of the IMF and the age are related to the random errors of the colors of the test models and the number of input parameters. A special series of numerical simulations is used to demonstrate the possibility of using the deviation functional to determine the interstellar extinction and the fraction of Lyman photons that do not contribute to the ionization of gas in a star-forming complex. The simulation results can be used to assess the accuracy of the IMF parameters and ages of young star-forming complexes based on the observational data available.

PACS numbers : 97.10.Bt, 98.20.Fk, 98.35.Ac, 98.62.Ai
DOI: 10.1134/S1063772907030055

1. INTRODUCTION

Determining the internal theoretical parameters of evolutionary models for star clusters based on their observed characteristics represents an inverse problem in astrophysics—in particular, the inverse star-formation problem. The desired quantities are the parameters of the initial mass function (IMF) of the cluster stars and the star-formation mode (history). The observed quantity is the stellar spectral energy distribution (SED) of the cluster, e.g., the integrated color indices derived from multicolor $UBVR$Hα photometry of star-forming complexes (SFC) in which the clusters themselves are embedded. If the IMF of forming stars and the history of the star-formation rate (SFR, i.e., the rate and mode of star formation) are known, then the direct problem, i.e., determining the SED of the star cluster at any time, has an unambiguous solution. By varying the parameters of the IMF, SFR, and age, we can select an evolutionary model for the star cluster or synthesize the stellar content of the galaxy so that its integrated photometric quantities best fit the observed values for the real SFC or galaxy. This approach was implemented to interpret the observed characteristics of SFCs and galaxies using the methods of evolutionary population synthesis and empirical population synthesis, which date back to the middle of the 20th century and the works of Tinsley [1], Morgan [2], Wood [3], and Faber [4].

Both approaches associate variations of the observed photometric parameters of star clusters primarily with variations of their ages, extinctions, and chemical compositions for a specified IMF. See the recent papers [5, 6] for the history of the development of both approaches. The inverse problem of determining the IMF, age, and star-formation mode from the known SED of a star cluster reduces to searching for the minimum values of a deviation functional for the observed photometric parameters and their model values. The deviation functional is numerical function that assigns each evolutionary model a certain number characterizing the deviation of the observed photometric quantities from their model values. Since the model (synthetic) photometric parameters are functions of the desired physical parameters (IMF parameters and age), the deviation functional characterizes

†Deceased.

the closeness of the real IMF and age of the SFC to the evolutionary model. This is an ill-posed problem, and the solutions obtained are, in general, not unique [7].

This non-uniqueness is due to the multiparametric nature of the problem. Different combinations of internal physical parameters (IMF, age, SFR, and star-formation mode), and thus different star-cluster models at different stages of evolution, can have similar combinations of observed colors. As a result, two star clusters with very similar colors can correspond to widely separated minima of the deviation functional, i.e., to utterly different evolutionary models. Therefore, we not only searched for all local minima of the deviation functional, but also calculated their depths. The solution is then taken to be that for the deepest minumum.

Furthermore, to compute the deviation functional, we must correct the observed photometric quantities (integrated colors) for interstellar extinction of the stellar radiation. This procedure eliminates the age–extinction degeneration problem. We calculate the deviation functional each time using the chemical composition Z derived independently from spectroscopic observations of the ionized gas surrounding the star cluster in the SFC, thereby eliminating the age–metallicity degeneration [8].

Solving the inverse problem also requires computing evolutionary models for the star clusters. The main difference between the known methods of population synthesis and empirical population synthesis is that the latter involves directly searching for a solution of the star-formation problem: the model (synthetic) colors are calculated given the slope of the IMF, age, chemical composition, and interstellar extinction. The desired physical parameters are then varied to produce model colors that are close to their observed values. The parameters are varied until they yield model colors that are close to those for the observed SED of the star-forming region. The closeness is determined using the usual adopted criteria. The solutions are taken to be all combinations of age, extinction, and chemical composition that meet the adopted criteria. Recently, Cid Fernandes et al. [6] used the maximum likelihood method for the first time to choose the most probable solution.

The question of how variations of the observed colors are related to variations of the IMF parameters remains unexplored. Finding the solution to our problem involves searching for the deepest local minimum of the deviation functional, which is calculated for the entire domain of IMF parameters, ages, and star-formation modes for specified values of the interstellar extinction and chemical composition derived from observations. This enables us to avoid missing any possible solution (i.e., to find all local minima of the functional), take into account the relation between the variations of the star-cluster SEDs and IMF parameters, and avoid the age–extinction and age–metallicity degenerations. This approach also enables the use of any evolutionary models and any combination of observed quantities. The method is easy to implement when the target objects are young star-forming regions with uniform chemical compositions and simple stellar populations. Applying this approach to galaxies with complex stellar populations requires the use of a larger number of observed spectrophotometric quantities to reflect the multicomponent nature of the stellar population. Problems still remain, associated with allowance for inhomogeneity of the chemical composition and internal extinction in the galaxies. This reduces somewhat the reliability of the estimated physical parameters characterizing star formation in galaxies.

Nonetheless, Cid Fernandes et al. [5] recently investigated the star-formation problem used a deviation functional and the method of spectral synthesis to compare synthetic spectra with the observed spectra of about 50 000 galaxies (from the Sloan Digital Sky Survey) in the wavelength interval from 3650 to 8000 Å. However, this made use of a narrow spectrum of models. These authors use three evolutionary sequences with different chemical compositions but the same IMF, corresponding to the IMF for all the stars of the entire galaxy [9]. We have performed the computations reported here in order to investigate how accurately we can derive parameters of interest to us using a deviation functional in the case of young star-forming regions.

Section 2 briefly describes the evolutionary models calculated at the Institute of Astronomy of the Russian Academy of Sciences. Section 3 describes the method used to perform numerical simulations of test models in the absence of random errors in their colors. Section 4 shows the effect of random errors in the integrated colors on the accuracy of the estimated star-formation parameters. Section 5 describes numerical simulations investigating the fraction of Lyman photons that do not participate in ionization processes. Section 6 describes numerical simulation investigating extinction via minimization of the deviation functional. Section 7 compares the A_V values obtained using the deviation functional with those derived from spectroscopic observations of gas in the star-forming regions. Finally, Section 8 lists the main conclusions. We describe the method used to solve for star-formation parameters using a deviation functional in our earlier papers [10, 11].

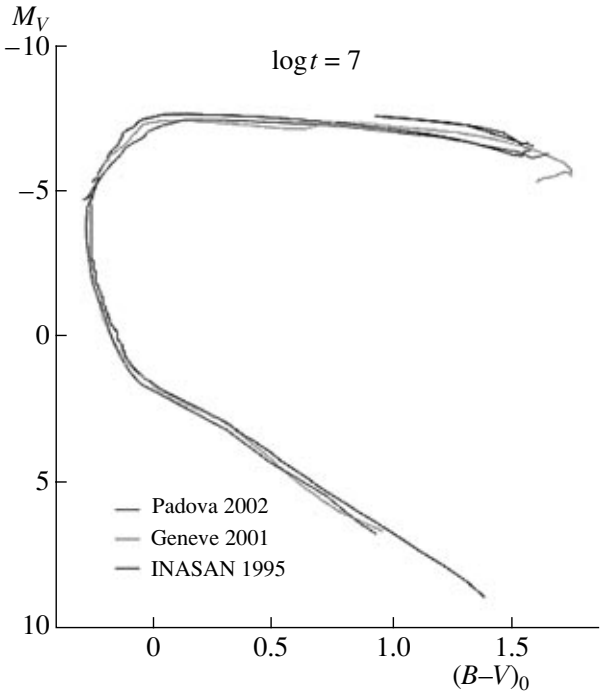

Fig. 1. Comparison of evolutionary tracks for a star cluster used by researchers at the Institute of Astronomy [12, 13], Lejeune and Schaerer [14], and Girardi et al. [15].

2. EVOLUTIONARY MODEL OF THE STELLAR POPULATOON OF A STAR-FORMING REGION

In this work, we used the cluster evolutionary model developed at the Institute of Astronomy of the Russian Academy of Sciences, described in detail in [12, 13]. Figure 1 compares the evolutionary tracks computed in these papers with the later evolutionary models of [14, 15].

We now briefly list the main characteristics of the model. We describe star formation using the function $b(m,t)$, which gives the number of stars N formed in unit mass interval dm over a unit time interval dt:

$$b(m,t) = \frac{d^2N}{dmdt}.$$

We assume a simple star-formation history in an individual young star-forming region, which we expect to contain stars of only one generation; this enables us to write $b(m,t)$ as the product of a function $f(m)$ describing the mass distribution of newly formed stars (the IMF) and a function $r(t)$ describing the intensity of star formation as a function of time (the SFR function):

$$b(m,t) = f(m)\cdot r(t).$$

We now adopt a power-law form for the IMF, $f \propto m^\alpha$, where the mass of newly formed stars is contained in the interval $m \in (M_{\min}, M_{\max})$; i.e., $M_{\min}$ and $M_{\max}$ are the lower and upper mass limits for the IMF. For $\alpha = -2.35$ we obtain the well-known Salpeter IMF [17].

We consider the following two cases for the SFR function $r(t)$.

(1) An Instantaneous Burst (IB) mode, where all stars of the cluster formed simultaneously t years ago. At time $t_0 = 0$ we have $r(t) = \delta(t_0)$.

(2) An Extended Burst (EB) mode, where star formation in the star-forming region began t years ago and has continued since then: $r(t) = \text{const}$.

The theoretical stellar composition of a star-forming region can be visualized graphically, e.g., on a color–color diagram (Fig. 2), or in the form of tabulated functions of integrated colors $U-B$, $B-V$, $V-R$, $\log(N_{\rm Lc}/L_B)$ as functions of the physical parameters of the model: the IMF slope α, upper mass limit $M_{\max}$, age t, chemical composition z, and star-formation mode $r(t)$:

$$\begin{aligned} U-B &= f_1(\alpha, M_{\max}, t, Z), \\ B-V &= f_2(\alpha, M_{\max}, t, Z), \\ V-R &= f_3(\alpha, M_{\max}, t, Z), \\ \log(N_{\rm Lc}/L_B) &= f_4(\alpha, M_{\max}, t, Z). \end{aligned} \quad (1)$$

We adopted the following variation intervals for the internal physical parameters:

$$\alpha \in (-0.35, -4.35), \quad M_{\max} \in (30, 120)M_\odot, \quad (2)$$
$$t \in (1, 100) \text{ million years}, \quad z \in (0.004, 0.040),$$
$$r(t) = \begin{cases} \delta(t), \\ \text{const}. \end{cases}$$

The tabulated functions of integrated colors $U-B$, $B-V$, $V-R$, and $\log(N_{\rm Lc}/L_B)$ computed with a specified step over the entire range of variation of α, $M_{\max}$, t, z, and $r(t)$ represent a multidimensional grid of evolutionary star-cluster models. The parameter steps were $h_\alpha = 0.05$ for the IMF slope, $h_{M_{\max}} = 30\ M_\odot$ for the upper mass limit of the IMF, and 0.1 on a logarithmic scale for the age. We computed for each chemical composition Z (known from observations) its own grid of evolutionary models. Every node of the grid represents a star-cluster model with a particular IMF, age, chemical composition, and star-formation mode.

We computed grids consisting of 648 evolutionary sequences. Every sequence contains models with ages ranging from 1–100 Myr. We limited the IB mode to an age of 20 Myr. The grid consists of a total of 13 284 nodes (models) for the specified chemical composition, including 5508 IB models nd 7776 EB models. Figure 2 shows a two-dimensional cross section of the grid (with a coarse step).

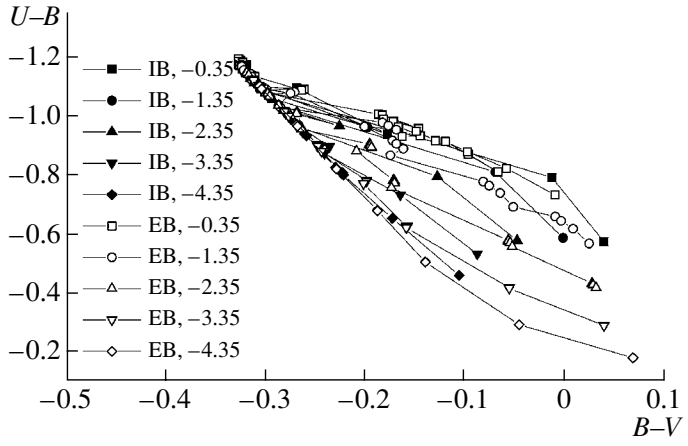

Fig. 2. Two-dimensional cross section of the Institute of Astronomy grid of evolutionary models. The steps in the IMF slope and age of the star-forming region are 1.0 and 0.2 dex, respectively. See text for notation.

3. NUMERICAL SIMULATIONS OF ESTIMATING THE IMF PARAMETERS AND AGE

If the chemical composition of the star-forming region is known, then, to unambiguously determine the four unknown physical characteristcs α, $M_{\max}$, t, and $r(t)$, we must know from observations four integrated color indices, e.g., $U-B$, $B-V$, $V-R$, and $\log(N_{\rm Lc}/L_B)$ [see relations (1)]. However, the observed colors are prone to measurement errors and interstellar extinction. The number of photons in the Lyman continuum can be calculated from the known fluxes in the Hα emission line. Since not all Lyman photons participate in ionization processes (some are absorbed by interstellar dust or simply leave the star-forming region), the fluxes in the Lyman continuum are underestimated. In view of this, we performed numerical simulations to model the solution process when the observed fluxes are subject to measurement errors and interstellar extinction.

The essence of the experiment is the following. We compute a test star-cluster model using a specified IMF slope α, IMF upper limit $M_{\max}$, age t, star-formation mode (IB or EB), and chemical composition Z. We then calculated the synthetic (i.e., input) color indices $(U-B)_{input}$, $(B-V)_{input}$, $(V-R)_{input}$, and $\log(N_{\rm Lc}/L_B)_{input}$ for this model, which we then "spoiled" with randomly distributed errors Δ_{U-B}, Δ_{B-V}, Δ_{V-R}, and $\Delta_{N_{\rm Lc}/L_B}$:

$$\begin{aligned}(U-B)_{exper} &= (U-B)_{input} + \Delta_{U-B}, \qquad (3)\\ (B-V)_{exper} &= (B-V)_{input} + \Delta_{B-V},\\ (V-R)_{exper} &= (V-R)_{input} + \Delta_{V-R},\\ \log(N_{\rm Lc}/L_B)_{exper} &= \log(N_{\rm Lc}/L_B)_{input} + \Delta_{N_{\rm Lc}/L_B}.\end{aligned}$$

We then compared these "distorted" color indices with the grid of evolutionary models by computing the deviation functional $F_{i,j,k}$ at each of the 13 284 grid nodes:

$$F_{i,j,k} = \sqrt{\sum_{l=1}^{3}\left[(\mathrm{O-C})_l^{i,j,k}\right]^2}, \qquad (4)$$

where

$$\begin{aligned}(\mathrm{O-C})_1^{i,j,k} &= (U-B)_{exper} - (U-B)_{table}^{i,j,k}, \qquad (5)\\ (\mathrm{O-C})_2^{i,j,k} &= (B-V)_{exper} - (B-V)_{table}^{i,j,k},\\ (\mathrm{O-C})_3^{i,j,k} &= (V-R)_{exper} - (V-R)_{table}^{i,j,k},\\ (\mathrm{O-C})_4^{i,j,k} &= \log(N_{\rm Lc}/L_B)_{exper}\\ &\quad - \log(N_{\rm Lc}/L_B)_{table}^{i,j,k}.\end{aligned}$$

The superscripts i, j, and k denote the node corresponding to $\alpha(i)$, $\log(t(j))$, $M_{\max}(k)$ of the model grid of synthetic colors. We took every node of the model grid where the deviation functional did not exceed the accuracy of the color indices ($\leq 0.25^m$) to be a possible solution. Among all these possible solutions, we identified the node (model) corresponding to the deepest local minimum of the deviation functional. We considered the IMF parameters, age, and star-formation mode for this model to represent the desired solution.

Table 1 gives the results of the first series of simulations with no random errors added to the input colors of the test models, i.e., where we set in (1) $\Delta_{U-B} = \Delta_{B-V} = \Delta_{V-R} = \Delta_{N_{\rm Lc}/L_B} = 0$.

We performed these simulations for a total of 160 previously constructed test models uniformly covering the entire range of variations of the physical parameters [see (2)]. These include 64 IB models

Table 1. Results of simulations of estimating the IMF parameters and age using various combinations of integrated colors

No. of simulation	Color combination	r_α, %	σ_α	r_t, %	σ_t	$r_{M_{\max}}$, %	$\sigma_{M_{\max}}$	IB, %	EB, %
1	2	3	4	5	6	7	8	9	10
1	$U-B, B-V, V-R, \log(N_{\rm Lc}/L_B)$	95	0.34	99	0.07	70	24	83	94
2	$U-B, B-V, \log(N_{\rm Lc}/L_B)$	92	0.44	98	0.10	63	26	80	93
3	$U-B, B-V, V-R$	94	0.35	97	0.14	61	27	61	88

Table 2. Effect of random errors in the colors on the accuracy of derived IMF parameters and age

No. of simulation	Combination of colors	r_α, %	σ_α	r_t, %	σ_t	$r_{M_{\max}}$, %	$\sigma_{M_{\max}}$	IB, %	EB, %	σ_{error}
1	2	3	4	5	6	7	8	9	10	11
1	$U-B, B-V, V-R, \log(N_{\rm Lc}/L_B)$	68	0.82	93	0.22	54	30	64	85	0.05^m
2	$U-B, B-V, V-R, \log(N_{\rm Lc}/L_B)$	68	0.85	92	0.24	50	31	61	79	0.10
3	$U-B, B-V, V-R, \log(N_{\rm Lc}/L_B)$	61	0.86	88	0.29	46	32	55	79	0.15
4	$U-B, B-V, \log(N_{\rm Lc}/L_B)$	40	1.02	88	0.32	10	38	62	79	0.05
5	$U-B, B-V, V-R$	66	0.84	90	0.25	14	37	42	66	0.05

and 96 EB models. In the first simulation of this series, we used all four integrated colors (Table 1, column 2). One or several colors are often lacking in the observational database, and, in some cases, only the Lyman continuum to B-band flux ratio is available. This is why we performed simulations 2 and 3 in order to determine the accuracy of the solution based on three integrated colors.

Columns 3 and 4 of Table 1 show that the correlation coefficient between the inferred and input IMF slopes is 92–95% for various star-formation modes and combinations of input colors, with the standard error of the IMF slope lying in the interval $\sigma_\alpha = 0.34-0.44$. In our previous paper [10], we use the method of pairwise comparisons to estimate the error of the slope to be $\sigma_\alpha \approx 0.50$.

Columns 5 and 7 give the correlation coefficients between the computed and input ages t and between the computed and input IMF upper limits $M_{\max}$, while Columns 6 and 7 give the standard errors of t and $M_{\max}$. It is immediately obvious that the correlation coefficient between the input and computed ages is high. The standard error of the inferred age lines in the interval $\sigma_{\log t} = 0.07-0.14$. The standard error of the age inferred from the integrated colors with observational errors is $\sigma_{\log t} = 0.29$. The derived IMF upper mass limit has a much lower accuracy; the correlation coefficient between the computed and input values is $r_{M_{\max}} = 60-70\%$, while the corresponding standard error is $\sigma_{M_{\max}} \approx 25\ M_\odot$. Figure 3 shows the relations between the computed and input IMF slopes and ages.

Columns 9 and 10 of Table 1 give the percentage of cases with incorrectly determined star-formation modes. It is obvious that the results for the instantaneous-burst (IB) mode (column 9) are sensitive to the presence of Lyman-continuum flux, $\log(N_{\rm Lc}/L_B)$, in the input data. Without this quantity, the fraction of correctly identified IB modes decreases from 83% down to 61%.

4. EFFECT OF RANDOM ERRORS OF THE INTEGRATED COLORS ON THE ACCURACY OF THE DERIVED IMF PARAMETERS AND AGE

In this series of simulations, we added randomly distributed errors to the integrated colors of the test models. We performed three simulations, with different dispersions for the distribution of random errors (Table 2, column 11). Random errors with $\sigma_{error} = 0.05$ correspond to the formal accuracy of the CCD photometry of 127 star-forming regions in the galaxy NGC 628 reported in our paper [17]. Table 2 summarizes the results of these computations.

In the first three simulations of this series, we compare the accuracy of the inferred quantities and the correlations between the input and inferred values for various random errors. It is obvious from Table 2

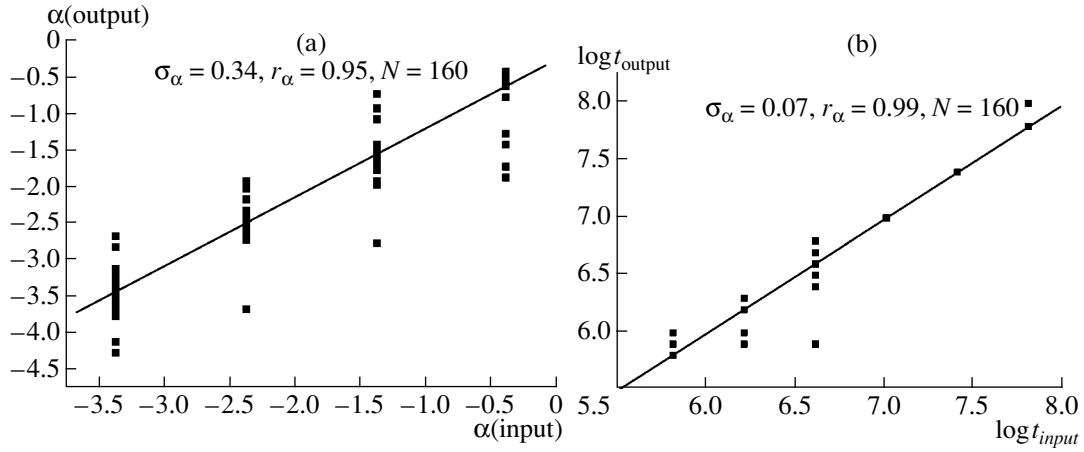

Fig. 3. (a) Computed IMF slope vs. input IMF slope and (b) computed vs. input age of the star-forming region.

that, as the random errors of the color indices increase, the correlation coefficients between the inferred and input quantities (for the IMF slope and age) decrease, and the standard errors increase. The estimated upper mass limits $M_{\max}$ remain unreliable even when the random errors correspond to those for the formal errors of the actual CCD photometry of [17]. We used simulations 4 and 5 (Table 2) to estimate the resulting accuracy of the solution based on three integrated colors in the presence of random errors. Here, the correlation coefficient between the inferred and input IMF slopes varies from 60% to 75%. The standard error of the IMF slope remains high: $\sigma_\alpha \approx 0.90$. The ages are determined fairly confidently, with the correlation coefficient between the inferred and input values ranging from 80% to 90% and a standard error of $\sigma_{\log t} = 0.2{-}0.3$. The estimates of the upper mass limit based on only three colors including random errors remain unreliable.

5. NUMERICAL SIMULATIONS OF THE FRACTION OF LYMAN PHOTONS THAT DO NOT PARTICIPATE IN IONIZATION PROCESSES

The number of Lyman-continuum photons emitted by the cluster stars is usually estimated from the observed Balmer-line flux of the cluster HII regions. However, a considerable fraction of Lyman-continuum photons does not take part in gas ionization, and the number of Lyman-continuum photons emitted by stars is therefore underestimated, on average, by 30–50% [19, 20]. The lack of reliable estimates of the fraction $1-f$ of Lyman-continuum photons not participating in ionization of the gas surrounding the cluster hinders us from using $\log(N_{\rm Lc}/L_B)$ when finding out solutions. Knowledge of the fraction $1-f$ of "missing" Lyman-continuum photons is in itself of interest for studies of the physics of star-forming regions, and we accordingly simulated estimation of this quantity using the deviation functional.

In the first step of the simulations, we decreased the Lyman-continuum fluxes $L_{N_{\rm Lc}}$ by $1-f = 50\%$ when computing the deviation functional $F_{i,j,k}$ (4) for the colors of the test model (3). We then searched for the minimum of the deviation functional with this artificially reduced Lyman flux. In the second step of the simulations, we reduced the Lyman-continuum fluxes $L_{N_{\rm Lc}}$ by $1-f = 45\%$ and again determined the minimum of the deviation functional. We further decreased the fraction of missing photons at each step by an additional 5% and determined the corresponding minima of the deviation functional. We took the initial value of $1-f$ to be that corresponding to the deepest minimum of the functional $F_{i,j,k}(1-f)$. In the exact solution, the deepest minimum of $F_{i,j,k}(1-f)$ should correspond to $1-f=0$. The deviation from zero constitutes the error in $1-f$. If the process yielded $1-f \neq 0$, we performed the second and subsequent iterations in the neighborhood of the $1-f$ value found at each iteration. We performed each subsequent iteration with step that has half as large, $h_{1-f}(i+1) = h_{1-f}(i)/2$, until $(1-f)_{i+1} \approx (1-f)_i$. The process nearly always converged by the third iteration. Table 3 gives the results of this series of simulations.

It is clear from Table 3 that the standard error in the fraction of missed photons is $\sigma_{1-f} = 11\%$ (column 4). When the color indices are subject to random errors, the error increases to $\sigma_{1-f} = 25\%$. In this case, the restored $\log(N_{\rm Lc}/L_B)$ ratios have standard errors $\sigma_{\log(N_{\rm Lc}/L_B)} = 0.22$ (Fig. 4). The correlation coefficient between the inferred and model values is $r_{\log(N_{\rm Lc}/L_B)} = 95\%$.

Table 3. Results of simulations of estimating the fraction $1-f$ of Lyman photons not participating in ionization processes

No. of simulation	Combination of colors	σ_{error}	σ_{1-f}, %	$r_{N_{\rm Lc}}$, %	$\sigma_{N_{\rm Lc}}$	r_α, %	σ_α	r_t, %	σ_t	IB, %	EB, %
1	2	3	4	5	6	7	8	9	10	11	12
1	$U-B$, $B-V$, $V-R$, $\log(N_{\rm Lc}/L_B)$	0.00^m	11	95	0.21	93	0.40	99	0.09	80	88
2	$U-B$, $B-V$, $V-R$, $\log(N_{\rm Lc}/L_B)$	0.05	25	95	0.22	66	0.84	92	0.24	48	77
3	$U-B$, $B-V$, $\log(N_{\rm Lc}/L_B)$	0.05	25	94	0.23	67	0.83	91	0.24	42	78

Table 4. Results of simulations of estimating the interstellar extinction

No. of simulation	Combination of colors	σ_{error}	r_{A_V}, %	σ_{A_V}	r_α, %	σ_α	r_t, %	σ_t	IB, %	EB, %
1	2	3	4	5	6	7	8	9	10	11
1	$U-B$, $B-V$, $V-R$, $\log(N_{\rm Lc}/L_B)$	0.00^m	99	0.12^m	76	0.69	88	0.27	47	82
2	$U-B$, $B-V$, $V-R$, $\log(N_{\rm Lc}/L_B)$	0.05	98	0.20	72	0.70	80	0.33	61	79
3	$U-B$, $B-V$, $V-R$	0.05	98	0.22	68	0.80	78	0.30	36	74

6. NUMERICAL SIMULATIONS OF ESTIMATING THE EXTINCTION USING A GRID OF EVOLUTIONARY MODELS

"Contaminating" the colors of our test models described by relations (3) by adding random extinctions $A_V(input)$ yields

$$\begin{aligned}(U-B)_{exper} &= (U-B)_{input} + \Delta_{U-B} \\ &+ E_{U-B}(input),\end{aligned} \quad (6)$$

$$\begin{aligned}(B-V)_{exper} &= (B-V)_{input} + \Delta_{B-V} \\ &+ E_{B-V}(input),\end{aligned}$$

$$\begin{aligned}(V-R)_{exper} &= (V-R)_{input} + \Delta_{V-R} \\ &+ E_{V-R}(input),\end{aligned}$$

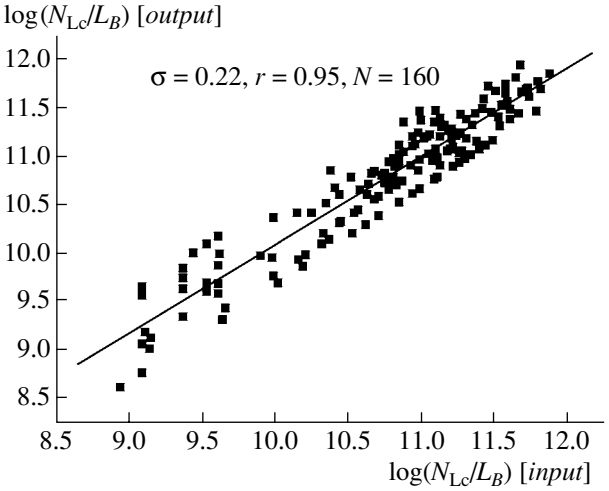

Fig. 4. Computed vs. input Lyman index.

$$\begin{aligned}\log(N_{\rm Lc}/L_B)_{exper} &= \log(N_{\rm Lc}/L_B)_{input} \\ &+ \Delta_{N_{\rm Lc}/L_B} + 0.4E_{{\rm H}_\alpha-B}(input),\end{aligned}$$

where the color excesses $E_{U-B}(input)$, $E_{B-V}(input)$, $E_{V-R}(input)$, and $E_{{\rm H}_\alpha-B}(input)$ are set by the random value $A_V(input)$ of the interstellar extinction in the V band in accordance with the formulas

$$\begin{aligned}E_{U-B}(input) &= A_U(input) - A_B(input) \\ &= (E_U - E_B)A_V(input),\end{aligned}$$

$$\begin{aligned}E_{B-V}(input) &= A_B(input) - A_V(input) \\ &= (E_B - E_V)A_V(input),\end{aligned}$$

$$\begin{aligned}E_{V-R}(input) &= A_V(input) - A_R(input) \\ &= (E_V - E_R)A_V(input),\end{aligned}$$

$$\begin{aligned}E_{{\rm H}_\alpha-B}(input) &= A_{{\rm H}_\alpha}(input) - A_B(input) \\ &= (E_{{\rm H}_\alpha} - E_B)A_V(input).\end{aligned}$$

Here, E_U, E_B, E_V, E_R, and $E_{{\rm H}_\alpha}$ are the selective extinction coefficients for U, B, V, R and the wavelength of Hα, respectively.

In formulas (6), we contaminated the intrinsic colors of the test models with both random interstellar extinction and random errors Δ_{U-B}, Δ_{B-V}, Δ_{V-R}, and $\Delta_{N_{\rm Lc}/L_B}$.

We used a random-number generator to create normally distributed random values $A_V(input)$ with a mean and dispersion of 2.5 and 1.05, respectively (Fig. 5a). We chose the parameters of this normal distribution to cover the range of observed values of A_V. Here, we used the empirical relation between the

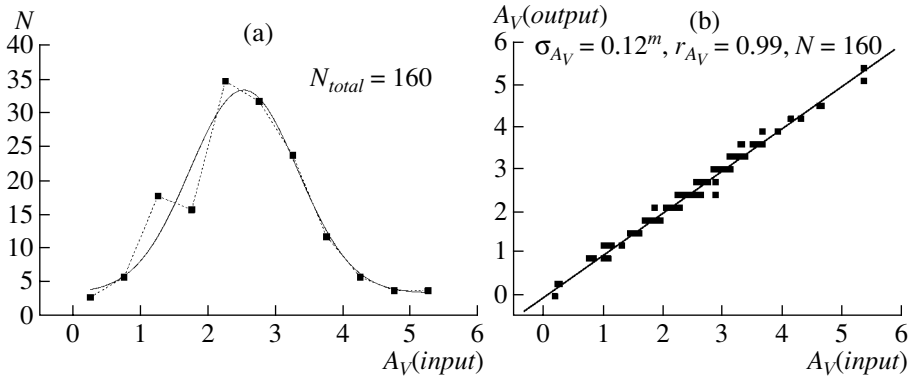

Fig. 5. (a) Distribution of input interstellar extinction $A_V(input)$ and (b) relation between the $A_V(input)$ and the computed interstellar extinction $A_V(output)$.

extinction in emission lines and in the stellar continuum derived in our earlier paper [20].

The aim of these simulations was to compute the output value $A_V(output)$ using the deviation functional, which, in the ideal case, would be equal to $A_V(input)$; i.e., we aimed to reconstruct the true colors of our test model.

Since $A_V(output)$ is not known a priori, we started the solution procedure with $A_V(output) = 0$ and continued to search for the minima of the deviation functional $F_{i,j,k}$ with an increment of $h_{A_V} = +0.1$ for all intermediate $A_V(output)$ values up to $A_V(output) = 5.5$. The initial value of the extinction was taken to be the value corresponding to the minimum of $F_{i,j,k}(A_V(output))$. This procedure was followed by second and third iterations in the neighborhood of the $A_V(output)$ value found at each iteration, which corresponded to the deepest minimum of the deviation functional (4). Each subsequent operation was performed with an increment half as large, $h_{A_V}(i+1) = h_{A_V}(i)/2$, until $A_V(output)^{i+1} \approx A_V(output)^i$. The process nearly always converged by the third iteration.

Table 4 lists the results of this series of simulations.

The first simulation (with zero color errors) shows a high correlation between the input and computed extinctions ($r_{A_V} = 99\%$; Table 4, column 4). The standard deviation of the computed extinctions (Table 4, column 5) is $\sigma_{A_V} = 0.12^m$, which corresponds to standard errors of 0.01^m–0.03^m in the reconstructed colors. Thus, determining the extinctions for the star-forming regions based on the grid of models developed at the Institute of Astronomy yields quite satisfactory results. Figure 5b compares the computed values $A_V(output)$ with the input extinctions $A_V(input)$.

However, real colors are subject not only to interstellar extinction, but also to observational errors. We repeated these numerical simulations including as well random errors in the input colors, corresponding to the formal accuracy of the measured integrated colors for the multicolor CCD photometry of [17]. In this case, the correlation between the computed and input extinctions remains high (98%), although the standard error increases to $\sigma_{A_V} = 0.20^m$. In the third experiment of this series, we used three color indices subject to random errors. The results remained virtually unchanged.

It is evident from Fig. 6 that the computed interstellar extinctions $A_V(output)$ are not correlated with the computed ages t_{output}. Thus the age–extinction degeneration does not arise when these quantities are determined using the deviation functional.

In this case, the method employed yields satisfactory age estimates, with a standard deviation of $\sigma_{\log t} = 0.22$–0.23. If random errors are added to the input colors, the standard error of the age increases to $\sigma_{\log t} \approx 0.30$. Applying the method of pairwise comparison to the ages estimated from the observed colors of real star-forming regions yielded approximately the same standard error, $\sigma_{\log t} = 0.29$ [10].

In the absence of independent measurements of interstellar extinction, the IMF slope is determined with an error of $\sigma_\alpha = 0.6$–0.8 and a correlation coefficient between the input and computed values of $r_\alpha = 60$–70%.

Figure 7 shows how much do the IMF upper mass limit, IMF slope, and age deviate from their true values if we do not correct the true input colors for interstellar extinction Δ_{A_V}. In this case, no effect of random errors is present. Note that $\Delta_{A_V} = \pm 0.30^m$ in the continuum corresponds to an extinction of $\Delta_{A_V}^{Balmer} = \pm 0.48^m$ in the hydrogen emission lines.

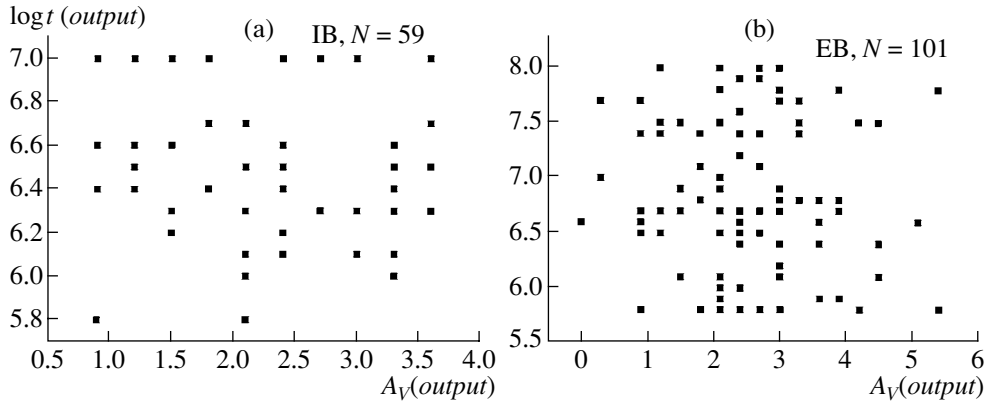

Fig. 6. Age vs. extinction for the (a) instantaneous-burst (IB) and (b) extended-burst (EB) star-formation modes.

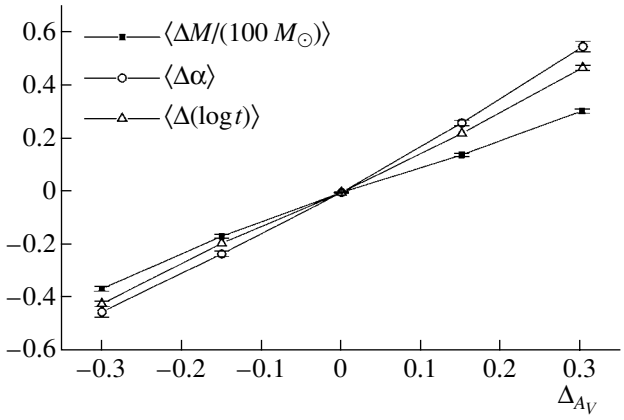

Fig. 7. Average deviations of the IMF parameters and age as a function of the error in the interstellar extinction Δ_{A_V}.

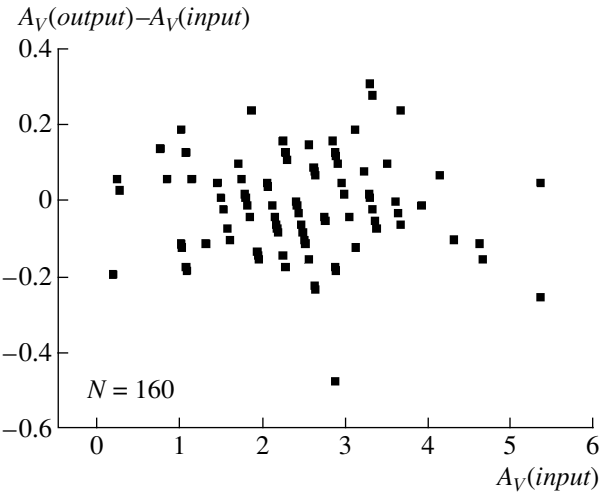

Fig. 8. Input interstellar extinction vs. accuracy of the extinction.

It is clear from Fig. 7 that underestimated extinction (colors that are too red) results not only in overestimated ages, but also affects the parameters of the IMF: the slope is systematically underestimated and the upper mass limit is overestimated. Here, we introduce the following notation:

$$\Delta M = M_{output} - M_{input}, \quad \Delta\alpha = \alpha_{output} - \alpha_{input},$$
$$\Delta(\log t) = \log t_{output} - \log t_{input}.$$

Figure 7 shows that the color variations should not be associated exclusively with variations of age and extinction. This approach results in incorrect determination of both the age and extinction.

As is obvious from Fig. 8, the accuracy of the derived extinction is independent of the extinction itself.

7. COMPARISON WITH OBSERVATIONS

We now apply this method for determining the extinction to real objects using available measurements of three colors and absorption in the Balmer lines. We will use the spectrophotometric observations of 99 HII regions in 20 galaxies obtained by McCall et al. [21]. McCall et al. [21] report estimates of the interstellar extinction in the Balmer lines, $A_V(Balmer)$ for these objects. In our earlier paper [22], we found data for at least three color indices for more than 40 objects in 12 galaxies in this sample. We compared the observed colors with a grid of evolutionary models to estimate the interstellar extinctions in star clusters located in these HII regions. Figure 9 compares the resulting "stellar" extinctions with the observed gas (Balmer) extinction.

The weakness of the correlation in Fig. 9 can be explained by the fact that the colors of the objects reported by McCall et al. [21] were not determined in the Johnson photometric system [23] in which the model colors are computed. We transformed the continuum

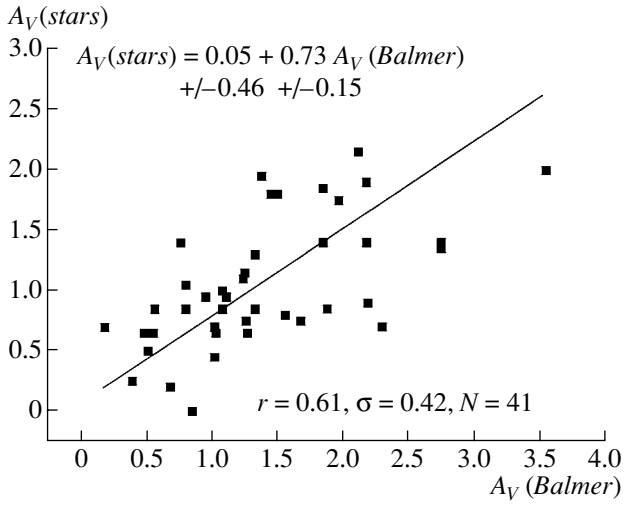

Fig. 9. Relation between the stellar extinction inferred by comparing the observed colors with a grid of evolutionary models and the gas extinction inferred from spectrophotometry of HII regions.

intermediate-band spectrophotometric observations of HII regions of [21] to standard Johnson colors using formulas for the linear interpolation of monochromatic logarithmic brightnesses [22]. The color transformation from the photometric system of [21] to the Johnson photometric system [23] yield standard errors of $\sigma_{U-B} = 0.11^m$ and $\sigma_{B-V} = 0.22^m$ for these color indices. The standard error of $V-R$ adopted from other sources is $\sigma_{V-R} \leq 0.15^m$. With these accuracies for the initial data, the standard error of the computed interstellar extinctions is $\sigma_{A_V} = 0.4^m$.

The second factor that reduces the correlation is that the relation between the extinction in the Balmer lines and in the stellar continuum depends on individual properties of the HII region. However, the overall form of the relation between the stellar and gas extinctions in Fig. 9 agrees, within the errors, with the corresponding relation for three galaxies obtained using a different method [20]:

$$A_V(stars) = (0.17 \pm 0.02) + (0.62 \pm 0.12) A_V(Balmer).$$

Cid Fernandes et al. [5] also obtained a similar relation between the stellar and gas extinctions.

8. CONCLUSIONS BASED ON THE RESULTS OF OUR NUMERICAL SIMULATIONS

Our numerical simulations of estimating the physical parameters characterizing star formation using a deviation functional based on the observed color indices showed that the deepest minimum of the functional corresponds, with satisfactory accuracy, to the true values of the desired IMF parameters, age, and star-formation mode. We have shown how the accuracy in the derived IMF, age, and star-formation mode depends on the random errors and the number and combination of input (observed) color indices. We used special numerical simulations (Section 5) to demonstrate the possibility of determining the fraction of Lyman photons that do not participate in the ionization of hydrogen, and thereby show that it is possible to determine the true Lyman-continuum flux based on the observed fluxes in Balmer lines. Of great practical importance are the results of our last series of simulations (Section 6), where we contaminated the test colors with random interstellar extinction and calculated the deviation functional for the entire range of variation of the physical parameters (the entire parameter space) and a wide range of interstellar extinctions. In this case, the deepest minimum of the functional corresponded to the random extinction value used to contaminate the true colors of the test model. We analyzed the well-known age–extinction degeneration, which did not arise in our adopted approach. Testing the method on real objects (Section 7) with known extinctions from independent spectroscopic observations demonstrated a satisfactory accuracy in A_V, which corresponds to the accuracy of the measured colors of the star-forming regions.

We generalize the results of the numerical simulations to demonstrate that the method employed reproduces the ages of star-forming regions well, much better than it reproduces the IMF parameters. Reliable estimates of the upper mass limit of the IMF can be obtained only from a nearly ideal set of observational data: four integrated colors corrected for interstellar extinction. The poor sensitivity of the method to the IMF upper mass limit is most likely due to the grid step, which was equal to 30 $M_\odot$. Imposing additional observational constraints, such as the empirical relation between the ages and sizes of star-forming regions [19, 22, 24], increases the accuracy of the derived IMF parameters. We will simulate the minimization of the deviation functional subject to observational constraints in a separate paper.

Mikhail Alexandrovich Smirnov died suddenly during the concluding stage of the preparation of the text of this paper. Mikhail Alexandrovich Smirnov was the first to suggest the use of methods from the calculus of variations to solve inverse problems in astrophysics in the middle 1980s. The emergence, development, and application of the method described in this paper is impossible to imagine without his encyclopedic knowledge and profound physical intuition. We feel deep sorrow at the irreparable loss of our colleague and friend.

ACKNOWLEDGMENTS

We are grateful to A.E. Piskunov (Institute of Astronomy of the Russian Academy of Sciences) for discussions of evolutionary models of star clusters. This work was partially supported by the Russian Foundation for Basic Research (project codes 04-02-16518, 05-02-16454, 06-02-16379, and 06-02-16857). F.Kh.S. acknowledges support from the ALDI Einkauf GmbH (Germany).

REFERENCES

1. B. M. Tinsley, Astrophys. J. **151**, 547 (1968).
2. W. W. Morgan, Publ. Astron. Soc. Pac. **68**, 509 (1956).
3. D. B. Wood, Astrophys. J. **145**, 36 (1966).
4. S. M. Faber, Astron. Astrophys. **20**, 361 (1972).
5. R. Cid Fernandes, A. Mateus, L. Sodre, Jr., et al., Monthly Not. R. Astron. Soc. **358**, 363 (2005).
6. R. Cid Fernandes, L. Sodre, H. Schmitt, and J. Leao, Monthly Not. Roy. Astron. Soc. **325**, 60 (2005).
7. A. V. Goncharskii, A. M. Cherepashchuk, and A. G. Yagola, *Chislennye Metody resheniya obratnykh zadach* (Numerical Methods for the Solution of Inverse Problems) (Nauka, Moscow, 1978) [in Russian].
8. A. Bressan, C. Chiosi, and R. Tantalo, Astron. Astrophys. **311**, 425 (1996).
9. G. Bruzual and S. Charlot, Mon. Not. R. Astron. Soc. **344**, 1000 (2003).
10. F. Sakhibov and M. A. Smirnov, Astron. Astrophys. **354**, 802 (2000).
11. F. Kh. Sakhibov and M. A. Smirnov, Astron. Zh. **78**, 3 (2001) [Astron. Rep. **45**, 1 (2001)].
12. A. E. Piskunov and V. I. Myakutin, Astron. Zh. **73**, 520 (1996) [Astron. Rep. **40**, 472 (1996)].
13. V. I. Myakutin, Astron. Tsirk. **1553**, 15 (1992).
14. Th. Lejeune and D. Schaerer, Astron. Astrophys. **366**, 538 (2001).
15. L. Girardi, G. Bertelli, A. Bressan, et al., Astron. Astrophys. **391**, 195 (2002).
16. E. E. Salpeter, Astrophys. J. **121**, 161 (1955).
17. V. V. Bruevich, A. S. Gusev, O. V. Ezhkova, et al., Astron. Zh. **84**, 253 (2007) [Astron. Rep. **51**, 222 (2007)].
18. M. Rozas, A. Zurita, and J. E. Beckman, Astron. Astrophys. **354**, 823 (2000).
19. F. Kh. Sakhibov and M. A. Smirnov, Astron. Zh. **81**, 998 (2004) [Astron. Rep. **48**, 909 (2004)].
20. F. Kh. Sakhibov and M. A. Smirnov, Astron. Zh. **72**, 318 (1995) [Astron. Rep. **39**, 281 (1995)].
21. M. L. McCall, P. M. Rybski, and G. A. Shields, Astrophys. J., Suppl. Ser. **57**, 1 (1985).
22. F. Kh. Sakhibov and M. A. Smirnov, Astron. Zh. **76**, 419 (1999) [Astron. Rep. **43**, 362 (1999)].
23. H. L. Johnson, Ann. Rev. Astron. Astrophys. **4**, 193 (1966).
24. Yi. N. Efremov and B. Elmegreen, Mon. Not. R. Astron. Soc. **299**, 588 (1998).

Translated by A. Dambis